Cerebellum (2008) 7:542–546
DOI 10.1007/s12311-008-0077-1

The Role of SK Calcium-Dependent Potassium Currents in Regulating the Activity of Deep Cerebellar Nucleus Neurons: A Dynamic Clamp Study

Steven Si Feng · Dieter Jaeger

Published online: 5 November 2008

Abstract We used the method of dynamic current clamping to determine the properties and function of the SK calcium-dependent K^+ current in neurons of the deep cerebellar nuclei (DCN). As previously reported, block of SK current with apamin leads to bursting of DCN neurons and a steepening of the f-I curve. We show here that the properties of the slow spike afterhyperpolarization are fully controlled by SK current and we derive kinetic properties of this current that explain its action on DCN neurons. Overall, the SK current provides an effective mechanism to tune the regularity of spiking and the f-I curve of DCN neurons.

Keywords Cerebellar nuclei · Rat · Action potential · Whole cell · Pacemaking · Calcium · Hyperpolarization

Introduction

Neurons in the deep cerebellar nuclei (DCN) are pacemakers in brain slice recordings when synaptic input is blocked [1] and fire spontaneously at a rate of about 10 Hz. This baseline may help explain their maintained activity in vivo despite a high level of inhibitory inputs from Purkinje cells. In DCN neurons the application of the specific SK calcium-dependent K^+ current blocker apamin leads to a dramatic shift from regular spiking to bursting and to a potent increase in spike rate with depolarizing current injection [2]. We further characterized the regulation of DCN spiking by SK current in this study using the method of dynamic current clamping.

S. S. Feng · D. Jaeger (✉)
Department of Biology, Emory University,
Atlanta, GA 30322, USA
e-mail: djaeger@emory.edu

Methods

Cerebellar Slices

Slices were obtained from Sprague-Dawley rats aged P15–P20. The animals were anesthetized with isofluorane and decapitated. The cerebellum was removed within 1 min and placed in an artificial cerebral spinal fluid (ACSF) consisting of (in mM) 124 NaCl, 3 KCl, 1.9 $MgSO_4$, 1.2 KH_2PO_4, 26 $NaHCO_3$, 2 $CaCl_2$, 20 glucose, bubbled with 95% O_2 and 5% CO_2 to a pH of 7.4. The cerebellum was then mounted on a vibratome and 300 μm-thick sagittal slices were made. The slices were incubated in ACSF at 32°C for at least 75 min before recording. All procedures were approved by the Emory IACUC and complied with the NIH Guide on Animal Use.

Electrophysiology

Cerebellar slices were placed in a recording chamber perfused with ACSF, containing 1 mM kynurenic acid (Sigma-Aldrich) and 100 μM picrotoxin (Sigma-Aldrich) to prevent synaptic transmission and maintained at 32°C. The slices were visualized using a Zeiss Axioskop microscope and DCN neurons were identified using a 60× water-immersion objective. Glass pipette electrodes were pulled from 1.5 mm borosilicate glass (Sutter Instruments, Novato, CA, USA) and were filled with an intracellular solution consisting of (in mM) 140 potassium gluconate, 6 NaCl, 10 HEPES, 0.2 EGTA, 2 $MgCl_2$, 0.05 spermine, 5 glutathione, 4 NaATP, 0.4 NaGTP. Whole cell patch clamp recordings

were performed using a Multiclamp 700B amplifier (Axon Instruments). To block SK current, 100 nM apamin (Sigma-Aldrich) and 1% bovine serum albumin were added to the perfusion solution. Current clamp recordings were sampled at 10 kHz using an NI PCI-6052E DAQ card (National Instruments, Austin, TX, USA) and custom data-acquisition software written in LabVIEW 8 (National Instruments).

Dynamic Current Clamp

Dynamic current clamp was used to add an artificial SK conductance to DCN neurons after exposure to apamin. Since the SK conductance is calcium-dependent, it was necessary to simulate a calcium pool and calcium inflow to this pool in real-time based on the voltage trajectory of the recorded neuron. The calcium inflow was carried by a voltage-dependent L-type calcium current (HVA) that we simulated with Hodgkin–Huxley kinetics and was linked in real-time to the voltage of the recording. An exponential outflow governed calcium decay and finally the SK current was determined using Hodgkin–Huxley kinetics and Hill equation-based calcium-binding activation from the resulting time course of simulated calcium concentration [3]. The equations used to instantiate the dynamic clamp real-time loop are listed in the appendix and were implemented with Labview 8.

Results

All neurons recorded (n=12, 9 animals) showed a dramatic effect of SK current block with 100 nM apamin on their baseline spiking (Fig. 1). The application of apamin lead to the disappearance of the slow spike afterhyperpolarization (sAHP), which had peak amplitudes that varied between 1 and 14 mV between neurons (Fig. 2b). There was a good exponential fit between the depth of the spontaneous sAHP and the spontaneous spike rate of neurons (r^2= 0.75), indicating that spike frequency was under the control of SK current. Neurons with a larger sAHP also showed a shallower f-I curve with positive current injection, indicating that responses to excitatory input were also regulated by SK current. The elimination of the sAHP with apamin lead to a pronounced bursting behavior in most neurons with inter-spike intervals (ISIs) during the burst that were far shorter than baseline ISIs (Fig. 1a,b). Some neurons showed depolarization block shortly after the onset of spiking in each burst or even permanently (not shown). In one neuron, a periodic up-state transition and plateau state was observed in the absence of spiking, indicating that burst profiles were not determined by spike currents. During the onset of apamin block a short period of irregular spiking in which short and long ISIs were intermixed was observed before the transition to full-fledged bursting (not shown).

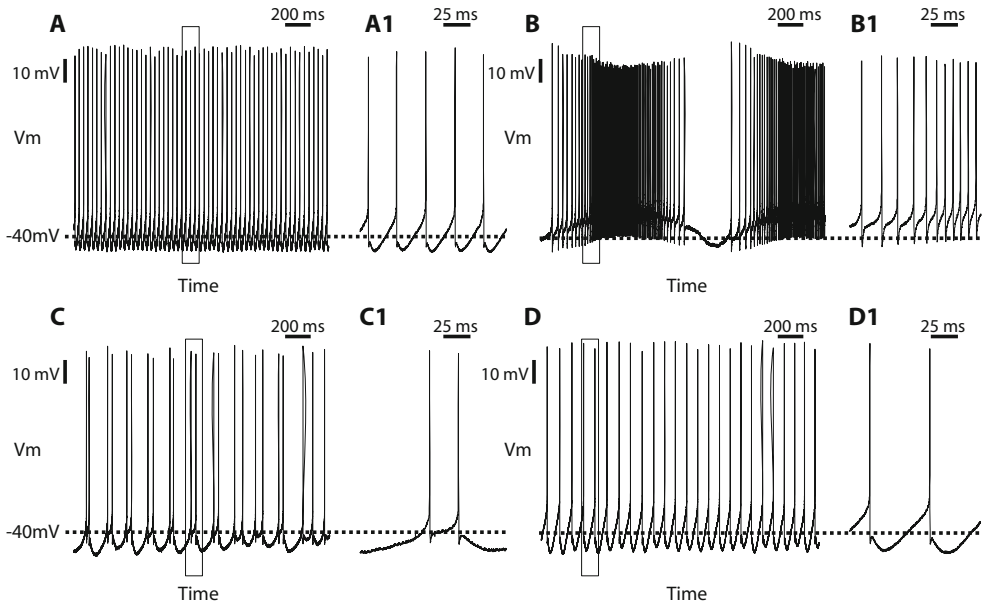

Fig. 1. Spike activity during baseline, apamin block, and recovered baseline conditions. **a** Regular baseline spiking at 19 Hz in this neuron. **a***1 Inset* of **a** showing the sAHP between spikes with an amplitude of 3 mV. **b** Bursting behavior after apamin block. **b***1 Inset* of **b** showing the absence of the sAHP and peak spike rate increase to 47 Hz. **c** Addition of a small amount of artificial SK current prevents bursting but results in irregular spiking. **c***1 Inset* of **c** showing that the superposition of artificial SK current following a brief ISI leads an enhanced sAHP and prolongation of the subsequent ISI. **d** Adding more artificial SK current leads to recovery of the regular baseline activity, although with a slower rate of 8.5 Hz and slightly deeper sAHP of 5 mV

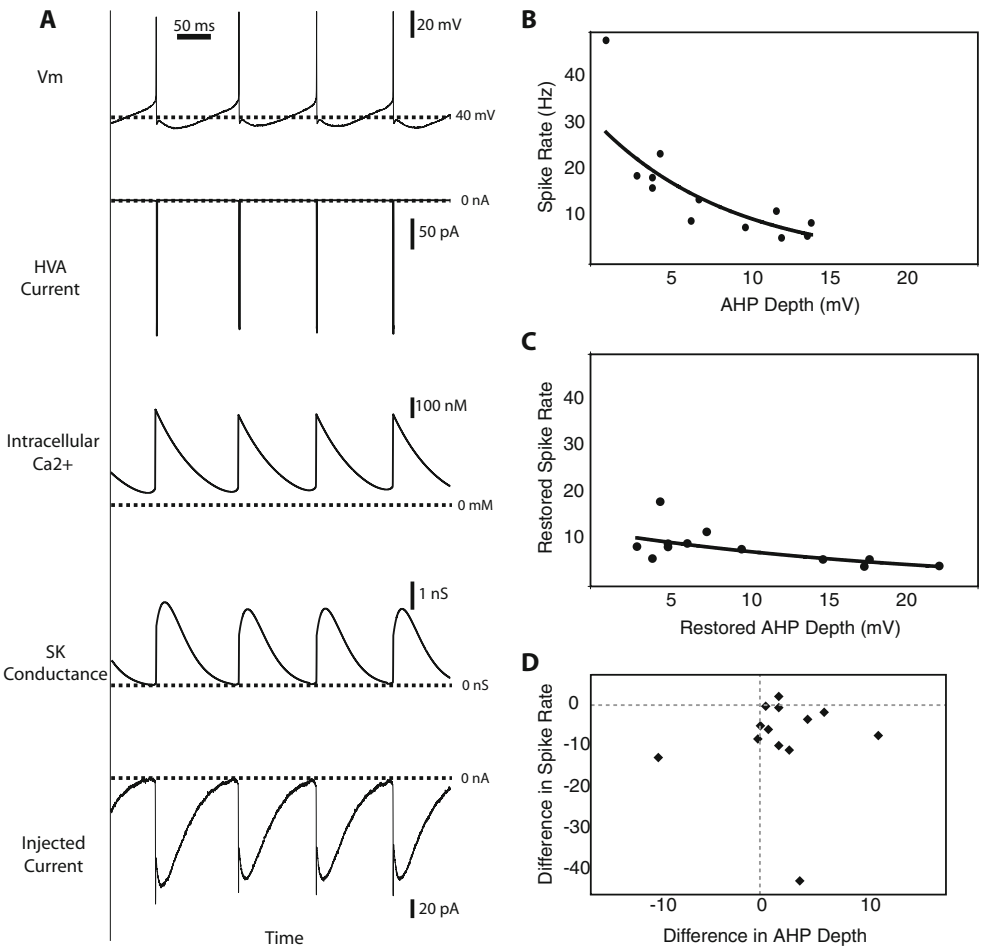

Fig. 2. Dependence of spike pattern on SK properties. **a** The dynamic clamp simulates a pulsatile HVA current with each spike with a subsequent calcium transient. This elicits an SK current underlying sAHP waveforms. **b** Exponential fit in the relationship between sAHP amplitude and spontaneous spike rate prior to SK block. **c** Recovery of this relationship after application of artificial SK current. **d** Relation between original and recovered sAHP and spike rates

We adjusted the parameters of an artificial SK current applied with dynamic clamping (see "Methods") within limits of known physiological properties to recover the baseline spiking of the neuron while endogenous SK current was blocked with apamin. This manipulation allowed us to 'titrate' the amount and time course of current needed to enable regular baseline spiking in each neuron. We found that a successful reconstitution of baseline spiking (Fig. 1d) was only possible with a SK current profile that had a fast onset after each spike, as otherwise spike doublets ensued (not shown). The decay time of SK current was dominated by the time course of calcium outflow. A calcium decay time constant between 20 and 30 ms was best suited to recover the time course of sAHPs. Since calcium decay has not been directly measured in DCN neurons, this value presents an experimentally testable prediction. Peak currents after each spike of the applied SK conductance ranged from 100 to almost 350 pA. For slow regular spiking SK current decayed back close to 0 before the next spike, but when ISIs were shorter (Fig. 1c), a superimposition of successive sAHP currents lead to an increase in amplitude. When the applied amplitude of artificial SK conductance was too small, this lead to irregular spiking (Fig. 1c) resembling the activity seen with partial SK block shortly after apamin application. Interestingly, the minimal amplitude of artificial SK current required to terminate irregular spiking was such that the ensuing sAHP had a slightly larger amplitude than seen during the original baseline activity (Fig. 2c,d). This lead to a slight slowing of the recovered regular spiking compared to the pre-apamin condition while maintaining a similar exponential fit in the relationship between sAHP amplitude and ISI duration for different neurons (r^2=54, Fig. 2b,c). This need for an increased amplitude of the artificial SK current could be explained by a spatial separation between our point of current injection (the soma) and the spike initiation zone (presumably the axon initial segment). With such a spatial separation a larger than baseline somatic AHP would be required in order to obtain sufficient hyperpolarization at the action initial segment due to passive sAHP decay. In contrast, endogenous SK current could be also operate directly at the point of spike initiation.

Discussion

We showed that the SK conductance in DCN neurons fully accounts for the sAHP in this cell type, and that this sAHP is a dominant factor in controlling spike frequency under baseline conditions and in response to current injection. A recent study showed that the SK current in DCN neurons is primarily due to inflow of HVA but not L-type calcium current [4]. Application of an artificial SK current with dynamic clamping using HVA current as a calcium source revealed that a pulsatile calcium inflow with each spike and a subsequent calcium decay with an approximate timing of 30 ms could explain the observed sAHP properties. This fast decay of intracellular calcium in the calcium pool may be representative of the short period of time that the SK channels are exposed to an elevated calcium concentration at the plasma membrane. The short exposure time may allow for the accumulation of intracellular calcium without the accumulation of SK current, which has been observed recently in sub-thalamic nucleus cells [5]. Furthermore, small differences in sAHP current amplitude had a significant impact on spike regularity, spike frequency, and f-I curves between DCN neurons, suggesting that regulation of the SK or HVA current through neuromodulation or activity-dependent plasticity affecting intracellular calcium dynamics [6] could be an important factor in controlling DCN spike patterns in vivo. An important influence of SK current on spike regularity has also recently been observed in cerebellar Golgi neurons and neurons in other brain structures [7–9], suggesting that SK current regulation could be a general mechanism of adjusting spiking patterns.

Appendix

Injected SK current:

$$I_{\text{inj}}(t) = \overline{g}_{\text{SK}} * n(t) * (E_K - V(t)) \tag{1}$$

Time dependence of SK conductance:

$$\frac{\partial n(t)}{\partial t} = \frac{n(t) - n_\infty(t)}{\tau_n(t)} \tag{2}$$

Calcium dependence of SK conductance:

$$n_\infty(t) = \frac{[Ca^{2+}](t)^4}{[Ca^{2+}](t)^4 + (0.0003)^4} \tag{3}$$

Time constant of SK conductance:

$$\tau_n = \begin{matrix} 0.06 - 11.2[Ca^{2+}](t) & [Ca^{2+}](t) > 0.005 \\ 0.004 & \text{otherwise} \end{matrix} \tag{4}$$

Calcium concentration:

$$\left[Ca^{2+}\right](t) = C(t) + \left[Ca^{2+}\right]_{\text{base}} \tag{5}$$

Calcium inflow and outflow:

$$\frac{\partial C(t)}{\partial t} = B * I_{\text{HVA}}(t) - \frac{C(t)}{\tau_{Ca}} \tag{6}$$

L-type calcium current:

$$I_{\text{HVA}}(t) = \overline{g}_{\text{HVA}} * m(t)^3 * (E_{Ca} - V(t)) \tag{7}$$

Activation gate of HVA current:

$$\frac{\partial m(t)}{\partial t} = \frac{m(t) - m_\infty(t)}{\tau_m(t)} \tag{8}$$

$$m_\infty(t) = \frac{1}{1 + \exp\left(\frac{V(t)+0.0345}{-0.009}\right)} \tag{9}$$

$$\tau_m(t) = Q_{\Delta T} \frac{0.1512}{a(t) + b(t)} \tag{10}$$

$$a(t) = \frac{1600}{1 + \exp(-72(V(t) - 0.005))} \tag{11}$$

$$b(t) = \frac{20(V(t) + 0.0089)}{\exp\left(\frac{V(t)+0.0089}{0.005}\right) - 1} \tag{12}$$

References

1. Gauck V, Jaeger D (2000) The control of rate and timing of spikes in the deep cerebellar nuclei by inhibition. J Neurosci 20(8):3006–3016, Apr 15
2. Aizenman CD, Linden DJ (1999) Regulation of the rebound depolarization and spontaneous firing patterns of deep nuclear neurons in slices of rat cerebellum. J Neurophysiol 82(4):1697–1709, Oct
3. Xia XM, Fakler B, Rivard A, Wayman G, Johnson-Pais T, Keen JE et al (1998) Mechanism of calcium gating in small-conductance calcium-activated potassium channels. Nature 395(6701):503–507, Oct
4. Alvina K, Khodakhah K (2008) Selective regulation of spontaneous activity of neurons of the deep cerebellar nuclei by N-type calcium channels in juvenile rats. J Physiol Lond 586(10):2523–2538, May
5. Teagarden M, Atherton JE, Bevan MD, Wilson CJ (2008) Accumulation of cytoplasmic calcium, but not apamin-sensitive

afterhyperpolarization current, during high frequency firing in rat subthalamic nucleus cells. J Physiol Lond 586(3):817–833, Feb
6. Yanovsky Y, Zhang W, Misgeld U (2005) Two pathways for the activation of small-conductance potassium channels in neurons of substantia nigra pars reticulata. Neuroscience 136(4):1027–1036
7. Forti L, Cesana E, Mapelli J, D'Angelo E (2006) Ionic mechanisms of autorhythmic firing in rat cerebellar Golgi cells. J Physiol Lond 574(3):711–729, Aug
8. Atherton JF, Bevan MD (2005) Ionic mechanisms underlying autonomous action potential generation in the somata and dendrites of GABAergic substantia nigra pars reticulata neurons in vitro. J Neurosci 25(36):8272–8281, Sep
9. Goldberg JA, Wilson CJ (2005) Control of spontaneous firing patterns by the selective coupling of calcium currents to calcium-activated potassium currents in striatal cholinergic interneurons. J Neurosci 25(44):10230–10238, Nov